arXiv:1408.0878v1 [astro-ph.SR] 5 Aug 2014

[Fe II] 1.64 μm Imaging Observations of the Outflow Features around Ultracompact H II Regions in the 1st Galactic Quadrant

Jong-Ho Shinn[1], Kee-Tae Kim[1], Jae-Joon Lee[1,2], Yong-Hyun Lee[3], Hyun-Jeong Kim[3], Tae-Soo Pyo[4], Bon-Chul Koo[3], Jaemann Kyeong[1], Narae Hwang[1], Byeong-Gon Park[1,2]

jhshinn@kasi.re.kr

ABSTRACT

We present [Fe II] 1.644 μm features around ultracompact H II regions (UCHIIs) found on a quest for the "footprint" outflow features of UCHIIs—the features produced by outflowing materials ejected during an earlier, active accretion phase of massive young stellar objects (MYSOs). We surveyed 237 UCHIIs in the 1st Galactic quadrant, employing the CORNISH UCHII catalog and UWIFE data, which is an imaging survey in [Fe II] 1.644 μm performed with UKIRT-WFCAM under $\sim 0.8''$ seeing condition. The [Fe II] features were found around five UCHIIs, one of which has low plausibility. We interpret the [Fe II] features to be shock-excited by outflows from YSOs, and estimate the outflow mass loss rates from the [Fe II] flux which are $\sim 1 \times 10^{-6} - 4 \times 10^{-5}$ $M_\odot$ yr^{-1}. We propose that the [Fe II] features might be the "footprint" outflow features, but more studies are required to clarify it. This is based on the morphological relation between the [Fe II] and 5 GHz radio features, the outflow mass loss rate, the travel time of the [Fe II] features, and the existence of several YSO candidates near the UCHIIs. The UCHIIs accompanying the [Fe II] features have relatively higher peak flux densities. The fraction of UCHIIs accompanying the [Fe II] features, 5/237, is small when compared to the ~ 90 % detection rate of high-velocity CO gas around UCHIIs. We discuss some possible explanations for the low detection rate.

Subject headings: ISM: jets and outflows — stars: formation — infrared: ISM — (ISM:) H II regions — surveys — shock waves

[1]Korea Astronomy and Space Science Institute, 776 Daeduk-daero, Yuseong-gu, Daejeon, 305-348, Korea

[2]Korea University of Science and Technology, 217 Gajeong-ro, Yuseong-gu, Daejeon, 305-350, Korea

[3]Dept. of Physics and Astronomy, Seoul National University, 1 Gwanak-ro, Gwanak-gu, Seoul, 151-742, Korea

[4]Subaru Telescope, National Astronomical Observatory of Japan, 650 North A'ohōkū Place, Hilo, HI 96720, U.S.A.

1. Introduction

The formation of massive stars ($M \gtrsim 8\,M_{\odot}$) is still unclear in many aspects (Zinnecker & Yorke 2007). One question to be resolved is how massive stars obtain their mass. It has been increasingly reported that, as in low-mass stars, the disk-mediated accretion process seems to be underway in forming massive stars (e.g. Beuther et al. 2002; Wu et al. 2004; San José-García et al. 2013; Cooper et al. 2013). However, it is still uncertain if disk accretion works in the mass range of $M \gtrsim 25\,M_{\odot}$ (Zinnecker & Yorke 2007).

One way to grasp the accretion process of massive young stellar objects (MYSOs) is by tracing the outflow features. In order for the massive (proto)star to accrete mass, the angular momentum of infalling material must be removed. If not, the angular momentum of infalling material would keep piling on the massive (proto)star, and the (proto)star would rotate in ever-increasing velocity. The outflow plays a significant role in removing this angular momentum (Lada 1985; Bachiller 1996), and produces outflow features in and around the MYSO. Therefore, by tracing these outflow features we can study the MYSO accretion history. In principle, we can study "early-stage" accretion activity even when the MYSO has already evolved to the "late-stage," using the outflow features.

Ultracompact H II regions (UCHIIs; size $\lesssim 0.1$ pc, density $\gtrsim 10^4$ cm^{-3}) are thought to be the late stage of MYSOs and no longer accreting significant mass (Churchwell 2002; Zinnecker & Yorke 2007). Since UCHII's natal clumps are not completely destroyed yet, one may expect that the materials ejected during the past, active accretion phase are still producing shocked features around the UCHIIs, colliding with the natal clump. In addition, shocked features can also be produced from the internal working surfaces of jets and outflows (Reipurth & Bally 2001; Arce et al. 2007). We will call these shocked features "footprint" outflow features, emphasizing the time difference between the current MYSO stage (i.e. UCHII) and the past MYSO stage when the outflowing material was launched. We thus expect high outflow mass loss rates from the "footprint" outflow features, since the outflowing material was launched during the past, active accretion phase.

These "footprint" outflow features are observable through radiative cooling lines, such as [Fe II] 1.64 μm, H_2 2.12 μm, and CO radio lines (Hollenbach & McKee 1989; Neufeld & Dalgarno 1989; Kaufman & Neufeld 1996; Wilgenbus et al. 2000; Flower & Pineau Des Forêts 2010). Indeed, CO outflow features have been observed around UCHII regions, such as G5.89-0.39 (Watson et al. 2007; Wood & Churchwell 1989), G18.67+0.03 (Cyganowski et al. 2012), G25.65+1.05 (Shepherd & Churchwell 1996), and G240.31+0.07 (Shepherd & Churchwell 1996). The dynamical timescale of these CO outflow features is $\gtrsim 10^4$ yr, which is comparable to the typical lifetime of UCHIIs ($\sim 4 \times 10^4$ yr, Wood & Churchwell 1989; González-Avilés et al. 2005) and MYSO jet-phase ($\sim 10^4 - 4 \times 10^5$ yr, Mottram et al. 2011;

Guzmán et al. 2012).

However, the CO outflow observations towards UCHIIs have been performed with low spatial resolutions greater than several arc seconds, limiting detailed study of accretion history, e.g. outflow morphology. Hence, [Fe II] line observations on the ground, whose typical seeing is $\sim 1.0''$, can be useful, although its capability for tracing outflows is limited by the depletion of Fe, and the requirements of high density and high shock velocity. The H_2 2.12 μm emission line is not useful for tracing outflow features around UCHIIs, which emit intense UV, because the emission line is easily excited by far-UV radiation (Hollenbach & Tielens 1997). We here present the [Fe II] 1.64 μm features around UCHIIs observed at a spatial resolution of FWHM $\sim 0.8''$. We employed the UKIRT imaging survey of the first Galactic quadrant in [Fe II] 1.64 μm, i.e. the UWIFE survey (Lee et al. 2014), with the UCHII catalog from the CORNISH survey (Hoare et al. 2012; Purcell et al. 2013). Among 237 UCHIIs, five UCHIIs were found to have nearby [Fe II] features, one of which had lower plausibility. We estimate the outflow mass loss rate from [Fe II] fluxes, and discuss whether the [Fe II] features can be the "footprint" outflow features. The relations between the [Fe II] detection rate and the UCHII parameters from the CORNISH catalog are also discussed.

2. Observations and Data Reduction

We used the [Fe II] imaging data from the UWIFE survey (Lee et al. 2014). This survey covers the 1st Galactic quadrant ($7^\circ < l < 63^\circ$, $|b| < 1.5^\circ$) using the [Fe II] 1.64 μm narrow-band filter. The [Fe II] filter was installed in the Wide-Field Camera (WFCAM, Casali et al. 2007) of the United Kingdom Infrared Telescope (UKIRT). The WFCAM provides four HgCdTe Rockwell Hawaii-II arrays (2048×2048), each of which has a field of view of $13.7' \times 13.7'$. These four arrays are located off-center, forming a square with a $12.9'$ gap. With this layout, observing at four discrete positions results in a contiguous area covering 0.75 deg^2 on the sky, i.e. a WFCAM tile.

The UWIFE survey were performed through 2012 and 2013, and the observed tiles are shown as gray shaded tiles in Figure 1. The two UCHIIs (G061.7207+00.8630 and G065.2462+00.3505) uncovered with the UWIFE survey were separately observed by targeting amid the 2013 campaign (14-Sep-2013). More on the observations is described in Lee et al. (2014).

Data reduction was implemented by the Cambridge Astronomical Survey Unit (CASU). The reduction process included dark subtraction, flat-fielding, bias subtraction, and sky correction. The details are described in Dye et al. (2006). The astrometric and photometric

calibrations (Hodgkin et al. 2009) were implemented employing the Two Micron All Sky Survey (2MASS) catalog (Skrutskie et al. 2006).

3. Analysis and Results

3.1. [Fe II] Feature Detection around UCHIIs

We searched for [Fe II] features around UCHIIs, using the candidate UCHII catalog of the CORNISH survey (Hoare et al. 2012; Purcell et al. 2013). The CORNISH survey was performed with the Very Large Array at 5 GHz over the 1st Galactic quadrant ($10^\circ < l < 65^\circ$, $|b| < 1^\circ$), which matches well with the coverage of our UWIFE survey (Fig. 1). The average beam sizes are $\sim 1.5''$ and $\sim 1.2''$ for the major and minor axes, respectively (Hoare et al. 2012). The catalog contains 240 sources, and we checked all the sources except three, which had no corresponding H-band image for continuum subtraction. The unchecked three UCHIIs are G025.3970+00.5614, G025.3983+00.5617, and G025.7157+00.0487. Figure 1 shows the distribution of CORNISH UCHII catalog sources plotted over the UWIFE survey coverage.

In order to find [Fe II] features, we used continuum-subtracted [Fe II] images and RGB composite images of [Fe II] and H (cf. Fig. 2 and 3). The H band images are from the UKIDSS Galactic Plane Survey (Lucas et al. 2008; Lawrence et al. 2007), and the continuum subtraction was done as described in Lee et al. (2014). We note that there is a time gap of a few years between the [Fe II] and H images. Therefore, time-variable continuum features can mimic [Fe II] features in the continuum-subtracted and RGB composite images mentioned above. This is more important considering that some UCHIIs show morphological changes on timescales of years (Acord et al. 1998; Franco-Hernández & Rodríguez 2004; van der Tak et al. 2005; Galván-Madrid et al. 2008), which suggests changes of the UCHII radiation environment.

We searched a $\sim 2.4' \times 2.4'$ area around the UCHII sources, and found five UCHIIs that had [Fe II] features around. We only picked the [Fe II] features not in contact with the 5 GHz radio features (cf. Fig. 2) in order to exclude [Fe II] features produced by the expanding H II regions. We also excluded pointlike [Fe II] features, since we cannot tell if they are variable stars or pointlike outflow features, due to the time gap between [Fe II] and H images mentioned above. These two types of excluded features are shown in Figure 4 as examples. Among the picked targets, we filtered out the UCHIIs whose [Fe II] features were less plausible, and named them 'candidates'. One of five selected UCHIIs is classified as a candidate. Figure 2 shows the UCHIIs accompanying [Fe II] features, while Figure 3 shows the candidate. The CORNISH 5 GHz image with a super-resolution of $\sim 1.5''$ (Purcell et al.

2013) is also shown for reference. More specific descriptions for individual objects are given below.

3.1.1. G025.3809−00.1815 and G025.3824−00.1812

Figure 2a shows the [Fe II] features around two UCHIIs: G025.3809-00.1815 and G025.3824-00.1812. These UCHIIs are also cataloged in Thompson et al. (2006). These two UCHIIs reside within the massive star cluster W 42, whose bright central star shows a MK type spectrum of O5–O6 (Blum et al. 2000). The [Fe II] features locate southwestward from the two UCHIIs, and show several knotty structures almost in a line pointing towards the two UCHIIs (cf. white dashed box of Figure 2a). We note here the diffuse southeast-northwest continuum features at the upper-left corner of the middle-left panel of Figure 2a, which locate in a symmetric position to the [Fe II] features with respect to the UCHIIs (see also Figure 7a). We can further trace the [Fe II] features closer to the two UCHIIs in the continuum-subtracted image, although its clear identification is hindered by strong diffuse continuum emissions and the crowded point sources near the two UCHIIs. The [Fe II] features show no overlap with the radio feature seen in the CORNISH 5 GHz continuum image, hence they seem to have no direct contact. We note that the 5 GHz morphology of G025.3809−00.1815 extends towards the [Fe II] features.

3.1.2. G028.2879−00.3641

Figure 2b shows the [Fe II] features around the UCHII G028.2879-00.3641. This UCHII is also cataloged in Kurtz et al. (1994) and Walsh et al. (1998). The environment of G028.2879-00.3641 is not crowded as much as G025.3809-00.1815 and G025.3824-00.1812. The [Fe II] features locate westward from the UCHII, showing an elongated shape (cf. white dashed box of Figure 2b). The elongated [Fe II] feature is stretched along the direction roughly perpendicular to the line connecting the UCHIIs and the [Fe II] features. It is hard to check if any [Fe II] feature exists near the UCHII, since diffuse continuum emissions are so strong. The [Fe II] features show no overlap with the radio feature seen in the CORNISH 5 GHz continuum image, hence they seem to have no direct contact. The 5 GHz morphology extends roughly along the direction to the [Fe II] features, as seen in G025.3809−00.1815.

3.1.3. G050.3152+00.6762 and G050.3157+00.6747

Figure 2c shows the [Fe II] features around two UCHIIs: G050.3152+00.6762 and G050.3157+00.6747. These UCHIIs are also cataloged in Wood & Churchwell (1989). The environment of the two UCHIIs is not crowded as much as G025.3809-00.1815 and G025.3824-00.1812. The [Fe II] features locate between the two UCHIIs at the northern part, and show knotty or elongated structures (cf. white dashed box of Figure 2c). The strong knotty feature seen in the continuum-subtracted image (near the upper-left corner of the white dashed box) also shows a pointlike feature in the H-band image. This [Fe II] feature could be a fake caused by the temporal variation of the point source as mentioned at the beginning of Section 3.1.

The elongated [Fe II] feature is stretched along the northeast-southwest direction. This [Fe II] feature resides at the northwestern edge of the UCHII G050.3157+00.6747 seen in the CORNISH 5 GHz continuum image. If the elongated [Fe II] feature is related with G050.3157+00.6747, they seem to have a direct physical contact; in this case, the [Fe II] feature is excluded from our examination, because we only picked [Fe II] features not overlapped with the 5 GHz radio feature (cf. see above). On the other hand, this elongated [Fe II] feature may be related with G050.3152+00.6762, since its stretching orientation is pointing towards G050.3152+00.6762, and G050.3157+00.6747 shows no [Fe II] feature along its edge except the northwestern edge. In that case, the elongated [Fe II] feature can be interpreted as a jetlike feature that has no direct contact with the UCHII. Unlike previous UCHIIs, the 5 GHz radio feature of G050.3152+00.6762 does not extend towards the [Fe II] features.

3.1.4. Candidate: G013.8726+00.2818

Figure 3 shows the [Fe II] features around the UCHII G013.8726+00.2818 (see the arrows). The [Fe II] features locate at the east, north, and northwest of the UCHII, showing extended shapes. The H-band image also shows similar extended features in the area of [Fe II] features. Therefore, the [Fe II] features could be fakes caused by the temporal variation of the extended continuum emissions; we thus classify this UCHII as a candidate. The [Fe II] features show no overlap with the crescent radio feature seen in the CORNISH 5 GHz continuum image, hence they seem to have no direct contact. The crescent shape of the UCHII is well matched with the dark lane seen in the RGB composite image, and extends roughly towards the [Fe II] features.

3.2. [Fe II] Flux Measurement and Extinction Correction

In order to characterize the physical quantity of the detected [Fe II] features, we measured their fluxes. The candidate [Fe II] features were excluded from the flux measurements, because they may not be real [Fe II] features. We picked some regions for measurement, which are shown on the right panels of Figure 2: on-source (*solid line*) and off-source (*dashed line*). Each region is labeled with a letter of the alphabet in order of increasing RA, and its position is listed in Table 1. For simplicity of the region name, we just picked one UCHII for the name prefix when there were two UCHIIs. The measured [Fe II] flux in each region is also listed in Table 1.

We then corrected the extinction effect on the measured [Fe II] flux employing the extinction curve of "Milky Way, R_V=3.0" (Weingartner & Draine 2001; Draine 2003). The amount of extinction was estimated by obtaining the total H column density ($N_{\rm H}$) from the color excess. The extinction and the corrected [Fe II] flux are listed in Table 1. The following sections describe how we obtained the extinction for the individual targets. The extinctions are $A_V \sim 9 - 20$, which is relatively small compared to the typical value of UCHIIs, $A_V \sim 30 - 50$ (Hanson et al. 2002).

3.2.1. G025.3809−00.1815 and G025.3824−00.1812

We adopted the color excess $E(H-K)$ estimated from the assumption that the massive stars of the cluster are on the main-sequence (Blum et al. 2000). The observed and intrinsic colors are $(H-K) = 0.637$ and $(H-K)_0 = -0.05$ in the CIT system, respectively. We used the effective wavelengths for Vega in the CIT system (Bessell & Brett 1988) in deriving the total H column density. A_{FeII} is about 1.64 mag.

3.2.2. G028.2879−00.3641

We estimated the color excess $E(H-K)$ using the UKIDSS photometry data (Lucas et al. 2008). We picked the point source which corresponds to the UCHII catalog position, and assumed that the extinction towards this source and the [Fe II] features were the same. The color of the picked UKIDSS source is $(H-K) = 0.556$. We assumed that this source was on the main-sequence, and adopted the intrinsic color of $(H-K)_0 = -0.04$ (Koornneef 1983). These two colors were compared in the 2MASS system, using the relations in Lucas et al. (2008) and Carpenter (2001). We used the isophotal wavelengths of the 2MASS system (Cohen et al. 2003) in deriving the total H column density. A_{FeII} is about 1.60 mag.

3.2.3. G050.3152+00.6762 and G050.3157+00.6747

We estimated the color excess $E(J-H)$ using the UKIDSS photometry data (Lucas et al. 2008). We picked two point sources which respectively correspond to the two UCHII catalog positions. The colors of the picked UKIDSS sources are $(J-H)=1.196$ for G050.3157+00.6747 and $(J-H)=2.054$ for G050.3152+00.6762, respectively. We used the mean value for the observed color. The color $(J-H)$ is used rather than $(H-K)$, because the UKIDSS photometry data do not provide the K-band photometry. We assumed that the two sources were on the main-sequence, and adopted the intrinsic color of $(J-H)_0=-0.13$ (Koornneef 1983). These two colors were compared in the 2MASS system, using the relations in Lucas et al. (2008) and Carpenter (2001). We used the isophotal wavelengths of the 2MASS system (Cohen et al. 2003) in deriving the total H column density. A_{FeII} is about 3.71 mag.

3.3. Excitation Mechanism for the [Fe II] Features

In this section, we examine the excitation mechanism for the observed [Fe II] features. We think the [Fe II] features are probably excited by shocks rather than UV radiation, as listed below. The shock driver is likely to be outflows from YSOs, because, in star forming regions, they are the most probable source generating supersonic motions that result in the observed [Fe II] features.

First, the [Fe II] features show different morphology from the diffuse near-infrared continuum features, which indicate the irradiated area[1]. The dominant UV radiation sources in the region are the massive stars ionizing the UCHIIs, and it is known that the [Fe II] emission well traces the warm neutral zone in the photo-dissociation regions (Burton et al. 1990). If the [Fe II] features are radiatively excited, they should show features similar to the continuum features. However, this is not the case (cf. Figures 2 and 5). Additionally, in the cases of G025.3809−00.1815, G025.3824−00.1812 (Figures 2a and 5a), and G028.2879−00.3641 (Figures 2b and 5b), there are continuum features that locate closer to the UCHIIs than the observed [Fe II] feature. These continuum features have no corresponding [Fe II] feature, which means the radiatively excited [Fe II] is weak. Therefore, the observed [Fe II] features have even less probability of being radiatively excited. We note that G050.3157+00.6747

[1]This near-infrared continuum is almost certainly dust-scattered light. It is not likely to be from thermal dust, since the temperature should be as high as $\sim 10^3$ K. This high dust temperature is not easy to achieve in the photo-dissociation region (cf. Hollenbach & Tielens 1997). Such a temperature is observed at supernovae (e.g. Fox et al. 2009).

(the left UCHII in Figure 2c and 5c) is excluded from this examination, because we only considered the link between G050.3152+00.6762 (the right UCHII in Figure 2c and 5c) and the [Fe II] feature (cf. section 3.1.3).

Second, the observed [Fe II] features locate far from the ionized regions, i.e. UCHIIs, as can be seen from the 5 GHz radio images (Figure 2). Therefore, the intensity of the hydrogen recombination line at the location of observed [Fe II] features would be low. Considering that the photo-ionized gas shows the line ratio of [Fe II]/Br$\gamma \simeq 0.1 - 2.5$ (Alonso-Herrero et al. 1997), the intensity of the photoionzed [Fe II] line would also be low at the location of the observed [Fe II] features.

3.4. Estimation of Outflow Mass Loss Rate

Based on the argument that the [Fe II] features are probably shock-excited by outflows from YSOs (cf. Section 3.3), we estimate the outflow mass loss rate ($\dot{M}_{out}$) from the [Fe II] flux (Table 1) in two different ways (cf. Section 3.2 of Shinn et al. 2013). We call them the "Fe-Shell" and "Fe-Stream" methods, respectively.

The "Fe-Shell" method assumes that the [Fe II] feature is excited by the wind shock and the ambient shock, both of which are J-type (for shock types, see Draine & McKee 1993), when the outflowing material is colliding with the ambient medium (cf. Fig. 3 of Shinn et al. 2013). We estimate $\dot{M}_{out}$ through the shock luminosity. The shock luminosity, which is expressed in terms of $\dot{M}_{out}$, is derived from the [Fe II] flux employing the shock model calculation. The "Fe-Stream" method assumes that the [Fe II] feature is a well-collimated stream of ionized gas flowing from the outflow source. We derive the total mass of the collimated medium from the [Fe II] flux, assuming the typical excitation condition of [Fe II] line. Then, we estimate the travel time from the measured outflow length and the assumed outflow velocity. From these mass and time values, we estimate $\dot{M}_{out}$.

We applied the "Fe-Shell" and "Fe-Stream" methods to the knotty and longish [Fe II] features, respectively. The "Fe-Stream" method is only applied to the [Fe II] feature in Figure 2c, relating it with the UCHII G050.3152+00.6762. The Fe depletion onto dust grains is also considered for both methods, in order to reflect the Fe depletion in jets (e.g. Beck-Winchatz et al. 1996; Mouri & Taniguchi 2000; Nisini et al. 2002, 2005; Podio et al. 2006; Giannini et al. 2008, 2013; Antoniucci et al. 2014). The logarithmic abundance of -4.63 (Allen et al. 2008), which is depleted by 0.13 dex (Asplund et al. 2009), is used for the "Fe-Shell" method. We apply the same depleted abundance for the "Fe-Stream" method, i.e. $A_{Fe/H} = 2.3 \times 10^{-5}$ (cf. eq (10) of Shinn et al. 2013). Table 2 lists the method used and the results, and $\dot{M}_{out}$

ranges $\sim 1 \times 10^{-6} - 4 \times 10^{-5}$ $M_{\odot}$ yr^{-1}.

In applying the "Fe-Shell" method to G025.3809−00.1815-B and G025.3809−00.1815-C (Figure 2a), we modify Eq. (8) of Shinn et al. (2013). These [Fe II] features have the corresponding H_2 $v = 1 \rightarrow 0$ $S(1)$ 2.12 μm features (Figure 5a), and the [Fe II] features probably come from the wind-shock only, rather than both wind and ambient shocks. We think the H_2 feature is likely from C-type shocks rather than J-type shocks, because only some of the observed [Fe II] features accompany the H_2 features. In this sense, the ambient shock is more likely to be C-type than the wind shock, since the ambient shock is propagating into a denser medium. Therefore, we modified Eq. (7) of Shinn et al. (2013) to be $L_{mech} = 1/2\, \dot{M}_{sw}\, v_{sw}^2$, and hence Eq. (8) of Shinn et al. (2013) is modified to $L_{mech} = 4/27\, \dot{M}_{out}\, v_w^2$. G028.2879−00.3641 has some filamentary H_2 features around it (Figure 5b), but its morphology is different from that of [Fe II] features (Figure 2b). We think this H_2 feature is probably excited by radiation, because it closely follows the near-infrared continuum features (cf. Section 3.3).

Table 2 also lists other physical parameters required for the $\dot{M}_{out}$ estimation. We adopted the outflow velocity of 200 km s^{-1}, because it falls within the typical outflow velocity of YSOs (Reipurth & Bally 2001) and the J-shock develops for a shock velocity of > 50 km s^{-1} under the typical cloud environments (Draine & McKee 1993; Le Bourlot et al. 2002). We adopted 100 km s^{-1} for G025.3809−00.1815-B and G025.3809−00.1815-C (Figure 2a and 5a), in order to make the ambient shock velocity slow enough to be C-type. The length scale and solid angle of the [Fe II] feature are from the ellipse used for the [Fe II] flux measurement (cf. Section 3.2). The distance to the individual UCHIIs was adopted as described in the following sections. We note that the $\dot{M}_{out}$ estimation includes the uncertainties that originate from several assumptions, such as the Fe depletion, the outflow velocity and the inclination (cf. Section 3.2.3 of Shinn et al. 2013).

3.4.1. G025.3809−00.1815 and G025.3824−00.1812

The kinematic distances to the cluster W 42 where the two UCHIIs reside were estimated as follows: 3.8 kpc (Anderson & Bania 2009), 3.92 kpc (Jones & Dickey 2012), 4.0 kpc (Kolpak et al. 2003), 5 kpc (Radhakrishnan et al. 1972), 10.8 kpc (Churchwell et al. 1990), 13.4 kpc (Wilson 1972), 13.5 kpc (Downes et al. 1980). The spectrophotometric distances were estimated to be 2.2 kpc (Blum et al. 2000) and 2.67 kpc (Moisés et al. 2011). The spectrophotometric distance suggests the UCHIIs probably locate at the near side among two ambiguous kinematic distances. Therefore, we adopted the distance of 3.9 kpc, which is the average of near-side distances estimated within ten years.

3.4.2. G028.2879−00.3641

The kinematic distances were estimated to be 3.0 kpc (Churchwell et al. 2010; Anderson & Bania 2009) and 3.29 kpc (Cyganowski et al. 2009). We adopted 3.2 kpc, averaging these values.

3.4.3. G050.3152+00.6762 and G050.3157+00.6747

The kinematic distances were estimated to be 2.1 kpc (Watson et al. 2003), 2.16 kpc (Araya et al. 2002), 8.7 kpc (Churchwell et al. 1990), and 9.7 kpc (Anderson & Bania 2009). The extinction to these UCHIIs are about $A_V \sim 20$, more than ten magnitude higher than other UCHIIs that locate at around $3-4$ kpc (Table 1). We think the distance of ~ 2.1 kpc is unlikely to give such a high extinction. Therefore, we adopted 9.2 kpc, averaging the two larger estimations.

3.5. UCHIIs with nearby [Fe II] Outflow Features and the CORNISH Catalog Parameters

In this section, we investigate the relations between the [Fe II] outflow features and the CORNISH catalog parameters (Table 3). First, we contrast the location of the UCHIIs accompanying [Fe II] features in the plots of three UCHII parameters: angular scale, integrated flux density, and peak flux density. These three UCHII parameters are from the CORNISH catalog (Purcell et al. 2013), and Figure 6 shows their scatter plots. The plot of angular scale versus integrated flux density presents a rough correlation (*black point*). This correlation seems to reflect the distance effect on the UCHIIs of semi-uniform luminosity and physical size, which should show (angular scale) $\sim$ (distance)$^{-1}$ and (flux) $\sim$ (distance)$^{-2}$, and hence (angular scale) $\sim$ (flux)$^{1/2}$. The plot of angular scale versus peak flux density presents almost no correlation. This seems to be caused by the weakening of the distance effect, replacing the integrated flux density with the peak flux density, which is likely independent of the distance.

The UCHIIs accompanying [Fe II] features occupy separate regions in Figure 6. This is more easily seen in the plot between peak flux density and angular size. The UCHIIs reside over the range of relatively higher peak flux density ($\sim 3\times10-1\times10^2$ mJy/Beam), regardless of angular scale.

3.6. Point Sources with Near-infrared Excess around UCHIIs

We are looking for the "footprint" outflow features around UCHIIs which were produced by the material ejected during the past, active accretion phase of MYSOs. However, considering that massive stars usually form in clusters, which include numerous other YSOs (Zinnecker & Yorke 2007, and references therein), the outflow features can also be produced by other YSOs. In order to examine the population of YSOs near the UCHIIs, we investigated the near-infrared color excess of nearby point sources.

Figure 7 shows the color-color diagram of $(J-H)$ versus $(H-K)$ and the corresponding composite image of H and [Fe II]. We use the photometry data from the UKIRT Infrared Deep Sky Survey (UKIDSS, Lawrence et al. 2007) Galactic Plane Survey (GPS, Lucas et al. 2008), except for G028.2879−00.3641. The UKIDSS GPS do not provide the J band photometry for G028.2879−00.3641, hence we instead used the photometry data from 2MASS (Skrutskie et al. 2006), which has inferior spatial resolution and survey depth to UKIDSS GPS (Lawrence et al. 2007). In the color-color diagram, we plot the locus of main-sequence stars employing the values in Hewett et al. (2006). For the 2MASS data, we transformed the locus using the equation in Hewett et al. (2006). The extinction line was calculated using the results of Rieke & Lebofsky (1985).

We classify the point sources that reside below the extinction line as showing the near-infrared excess. As Figure 7 shows, there are several point sources with near-infrared excess around UCHIIs. These sources could be YSOs, and they could potentially produce the [Fe II] outflow features observed around UCHIIs.

4. Discussion

4.1. Nature and Origin of the [Fe II] Features around UCHIIs

We seek the "footprint" outflow features around UCHIIs, which are produced by the material ejected during the prior, active accretion phase of MYSOs. The [Fe II] 1.644 μm emission line was employed, and we found that five out of 237 UCHIIs have nearby [Fe II] features. Based on the given observational facts and estimations, it seems that the detected [Fe II] features might be the "footprint" outflow features, but more detailed and targeted study is required to clarify it. More specific points are given below.

First, the morphological relation between the [Fe II] and 5 GHz radio continuum features is compatible with the "footprint" interpretation. The radio features are elongated towards the [Fe II] features in the cases of G025.3809−00.1815 (Figure 2a) and G028.2879−00.3641

(Figure 2b). The candidate G013.8726+00.2818 (Figure 3) also shows a similar morphological relation. Only G050.3152+00.6762 (Figure 2c) does not show such a relation. However, considering that the [Fe II] features near G050.3152+00.6762 could be produced by the other UCHII G050.3157+00.6747, all the facts suggest a relation between the [Fe II] and radio continuum features.

This morphological relation can be understood in the disk-accreting MYSO model (e.g. Yorke & Sonnhalter 2002; Krumholz et al. 2009; Kuiper & Yorke 2013a), which has a bipolar cavity excavated by the radiation pressure and outflow materials. The cavity structure is seen up to the radial distance of $\sim 2 \times 10^4$ AU ~ 0.1 pc, which is comparable to the typical size of a UCHII (Wood & Churchwell 1989; Hoare et al. 2007). The ionized gas would expand more rapidly through the cavity, hence the morphology of ionized gas would be extended along the cavity direction, i.e. the outflow direction. The diffuse near-infrared continuum features seen northeastward from G025.3809−00.1815 and G025.3824−00.1812 (Figure 2a) likely emanated through such a cavity. Also, the high-velocity CO gas mapped in the study of Shepherd & Churchwell (1996) are probably from the bipolar outflows following the cavity.

Second, $\dot{M}_{out}$ does not give a clear answer as to whether the [Fe II] features are the "footprint" outflow features or not. $\dot{M}_{out}$ is estimated to be $\sim 1 \times 10^{-6} - 4 \times 10^{-5}$ $M_\odot$ yr^{-1} (Table 2). If we assume a typical ratio between the outflow mass loss rate and the disk accretion rate $\dot{M}_{out}/\dot{M}_{acc}$=0.1 (Ellerbroek et al. 2013; Ray et al. 2007; Frank et al. 2014), we can guess $\dot{M}_{out}$ from $\dot{M}_{acc}$ of MYSO models. The $\dot{M}_{acc}$ of MYSO models ranges $\sim 10^{-4}-10^{-3}$ $M_\odot$ yr^{-1} (e.g. Yorke & Sonnhalter 2002; Krumholz et al. 2009, 2012; Kuiper & Yorke 2013b), hence $\dot{M}_{out}$ would be around $\sim 10^{-5} - 10^{-4}$ $M_\odot$ yr^{-1}. Our $\dot{M}_{out}$ estimation is overlapped with this model-inferred $\dot{M}_{out}$, but a little lower. Meanwhile, our $\dot{M}_{out}$ is comparable to the $\dot{M}_{out}$ of low- or intermediate-mass YSOs such as the Herbig Ae/Be star and FU Ori object (Ellerbroek et al. 2013). We therefore cannot exclude the possibility that the observed [Fe II] features were produced by nearby low- or intermediate-mass YSOs.

Third, the travel time of the [Fe II] features does not exclude the "footprint" interpretation, although the time is roughly estimated. If the outflow material that excites the [Fe II] features is ejected from the location of a UCHII, we can guess the time the material spent to arrive at the [Fe II] feature position. We adopted the velocity and the distance listed in Table 2, and assumed the outflow material flowing on the plane of the sky. The travel time is estimated to be $\sim (1 - 8) \times 10^3$ yr (Table 4). These times are shorter than the typical lifetime of UCHIIs ($\gtrsim 5 \times 10^4$ yr, Wood & Churchwell 1989; González-Avilés et al. 2005) and MYSO jet-phase ($\gtrsim 4 \times 10^4$ yr, Mottram et al. 2011; Guzmán et al. 2012). Therefore, depending on when the outflow was launched, the [Fe II] feature can be interpreted as the "footprint", or even as having been excited by the outflow launched *during* the UCHII phase.

We note that some studies assert there is the ongoing accretion onto the central object even after the H II region development (Keto 2002, 2003; Keto & Wood 2006; Keto & Klaassen 2008). For reference, we calculated the expansion time of UCHIIs (Table 4), using the typical sound velocity of the H II region and the deconvolved size of UCHIIs (Table 3). Both the expansion and travel times have a similar order of magnitude. The adopted sound velocity is $c_s = \sqrt{\gamma kT/\mu m_H} \sim 15$ km s^{-1} with $\gamma = 5/3$, $\mu = 0.61$, and $T = 10^4$ K. We note that the travel time can be longer if the inclination to the plane of sky is allowed for. The outflow velocity is definitely another element that can make the time shorter or longer.

Fourth, several YSO candidates existing near the UCHIIs hinder the "footprint" interpretation. As Figure 7 shows, there are several point sources that have near-infrared color excesses near the UCHIIs. If these sources are YSOs, they could have produced the observed [Fe II] features. For example, the YSO candidates close to the cataloged UCHII position could have (Figure 7a and b), and the YSO candidate at the northeast of G050.3152+00.6762 also could have (Figure 7c). The three points argued above—morphology, $\dot{M}_{out}$, travel time—can be understood without the "footprint" interpretation, if the YSO candidates near UCHIIs can produce $\dot{M}_{out}$ of $\sim 1 \times 10^{-6} - 4 \times 10^{-5}$ $M_\odot$ yr^{-1}, like the Herbig Ae/Be star or FU Ori objects (Ellerbroek et al. 2013). In that case, the travel time of $\sim (1 - 8) \times 10^3$ yr (Table 4) is not contradictory to the typical lifetime of a Herbig Ae/Be star (a few Myr, Waters & Waelkens 1998) or a FU Ori object (~ 0.1 Myr, Hartmann & Kenyon 1996).

4.2. [Fe II] Feature Detection and UCHII Parameter

Figure 6 shows that the UCHIIs accompanying [Fe II] features reside over the relatively higher range of peak flux density ($\sim 3 \times 10 - 1 \times 10^2$ mJy/Beam), regardless of the angular size. Considering that the peak flux density would decrease as the UCHII expands, this distribution indicates that the [Fe II] features are more likely produced around younger UCHIIs. This is reasonable, because younger UCHIIs would disperse less nearby natal clump materials and would increase the chance of collision between the outflow and natal clump materials.

Five out of 237 UCHIIs showed nearby [Fe II] features. For comparison, we note the $\sim 90\%$ detection rate of high-velocity CO gas around 94 UCHIIs observed in radio (Shepherd & Churchwell 1996). Also, Varricatt et al. (2010) detected H_2 features around four of 13 UCHIIs, imaging H_2 $\upsilon = 1 \rightarrow 0$ $S(1)$ 2.12 μm emission line. The H_2 $\upsilon = 1 \rightarrow 0$ $S(1)$ line is well excited by far-UV radiation (Hollenbach & Tielens 1997), hence we should be careful in interpreting these H_2 features as outflow features. If these H_2 features are outflow features, the overall CO, H_2, [Fe II] detection rates can be understood with the probability

distribution of outflow velocity. In order to be excited, CO, H_2, and [Fe II] require shock velocities of increasing magnitude. Therefore, if the outflow velocity distribution has a higher probability at a lower velocity, then the CO, H_2, [Fe II] detection rates of decreasing order can be explained.

One possible reason for the low [Fe II] detection rate is the extinction towards UCHIIs, which is typically $A_V \gtrsim 30-50$ (Hanson et al. 2002) $\sim A_H \gtrsim 6-9$ (Draine 2003). Therefore, we may miss numerous [Fe II] features. Note that A_V for three UCHIIs in Table 1 are relatively low ($A_V \sim 9-20$). Another possible reason is that the outflow cavity is already open to the outside of the natal clump (cf. Kim & Koo 2001), and hence less materials exist to collide with the outflow. The typical size of clumps ($\sim 0.3-3$ pc, Bergin & Tafalla 2007) is smaller than the traveling distance of a $100-200$ km s^{-1} outflow material over the typical lifetime of a MYSO jet-phase ($\gtrsim 4\times10^4$ yr, Mottram et al. 2011; Guzmán et al. 2012). If the outflow direction is steady, it would make the situation worse. Another possible reason is the weakness of [Fe II] features. The shocked [Fe II] feature are likely to be unresolved and the [Fe II] flux is proportional to the column density along the line of sight. Hence, weak [Fe II] features from low column density might not have been detected due to the detection limit. The UWIFE survey has a nominal 5-σ detection limit of ~ 18.7 mag for point sources (Lee et al. 2014). The low outflow velocity is another possible reason. If the outflow material is ejected with velocity too low to produce J-type shock (cf. Draine & McKee 1993; Le Bourlot et al. 2002) during a certain amount of time, e.g. low accretion duration, the chance of seeing the [Fe II] feature is reduced. Finally, if the outflow material is clumpy or bullet-like rather than continuous stream-like, then the chance to observe a shocked [Fe II] feature would be lower, depending on the emergence frequency of the outflow material. The observed [Fe II] features appear to be both stream-like (Figure 2c) and clumpy (Figure 2b) outflow materials. More observations for the weaker [Fe II] features would help in assessing the effects of outflow type on the [Fe II] feature detection.

5. Conclusions

We sought the "footprint" outflow features around UCHIIs which are produced by materials ejected during the past, active accretion phase of MYSOs. The UWIFE survey data (Lee et al. 2014) and the CORNISH UCHII catalog (Hoare et al. 2012; Purcell et al. 2013) were employed for the search. The UWIFE survey is an imaging survey of the [Fe II] 1.644 μm emission line, and the CORNISH survey is a 5 GHz radio continuum survey, both of which cover the 1st Galactic quadrant. The typical seeings of the two surveys are $\sim 0.8''$ (UWIFE) and $\sim 1.5''$ (CORNISH), respectively.

Five out of 237 UCHIIs showed nearby [Fe II] features, one of which was less plausible and was tagged as a candidate. We propose that these [Fe II] features might be the "footprint" outflow features we are searching for, but more detailed and targeted study is required to clarify it. This is based on the following observational facts and estimations: the morphological relation between the [Fe II] and 5 GHz radio features, $\dot{M}_{out}$ estimated from the [Fe II] flux, the travel time of the [Fe II] features, and the existence of several YSO candidates near the UCHIIs. The UCHIIs accompanying the [Fe II] features have a relatively higher peak flux density in 5 GHz. The fraction of UCHIIs accompanying the [Fe II] features, 5/237, is small compared to the $\sim$ 90 % detection rate of high-velocity CO gas around UCHIIs. We discuss the reasons for this low detection rate, including the extinction, the configuration of the outflow cavity, the weakness of [Fe II] features, the low outflow velocity, and the outflowing type. We note that the sub-arcsec interferometric observations of CO rotational lines would be useful in studying the "footprint" outflow features, considering its high detection rate.

J.-H. S. is grateful to Melvin Hoare and Stuart Lumsden for the discussion on the results. H.-J. K. was supported by NRF(National Research Foundation of Korea) Grant funded by the Korean Government (NRF-2012-Fostering Core Leaders of the Future Basic Science Program).

REFERENCES

Acord, J. M., Churchwell, E., & Wood, D. O. S. 1998, ApJ, 495, L107

Allen, M. G., Groves, B. A., Dopita, M. A., Sutherland, R. S., & Kewley, L. J. 2008, ApJS, 178, 20

Alonso-Herrero, A., Rieke, M. J., Rieke, G. H., & Ruiz, M. 1997, ApJ, 482, 747

Anderson, L. D., & Bania, T. M. 2009, ApJ, 690, 706

Antoniucci, S., La Camera, A., Nisini, B., et al. 2014, A&A, 566, A129

Araya, E., Hofner, P., Churchwell, E., & Kurtz, S. 2002, ApJS, 138, 63

Arce, H. G., Shepherd, D., Gueth, F., et al. 2007, Protostars and Planets V, 245

Asplund, M., Grevesse, N., Sauval, A. J., & Scott, P. 2009, ARA&A, 47, 481

Bachiller, R. 1996, ARA&A, 34, 111

Beck-Winchatz, B., Bohm, K.-H., & Noriega-Crespo, A. 1996, AJ, 111, 346

Bergin, E. A., & Tafalla, M. 2007, ARA&A, 45, 339

Bessell, M. S., & Brett, J. M. 1988, PASP, 100, 1134

Beuther, H., Schilke, P., Sridharan, T. K., et al. 2002, A&A, 383, 892

Blum, R. D., Conti, P. S., & Damineli, A. 2000, AJ, 119, 1860

Burton, M. G., Hollenbach, D. J., & Tielens, A. G. G. M. 1990, ApJ, 365, 620

Carpenter, J. M. 2001, AJ, 121, 2851

Casali, M., Adamson, A., Alves de Oliveira, C., et al. 2007, A&A, 467, 777

Churchwell, E. 2002, ARA&A, 40, 27

Churchwell, E., Sievers, A., & Thum, C. 2010, A&A, 513, A9

Churchwell, E., Walmsley, C. M., & Cesaroni, R. 1990, A&AS, 83, 119

Cohen, M., Wheaton, W. A., & Megeath, S. T. 2003, AJ, 126, 1090

Cooper, H. D. B., Lumsden, S. L., Oudmaijer, R. D., et al. 2013, MNRAS, 430, 1125

Cyganowski, C. J., Brogan, C. L., Hunter, T. R., & Churchwell, E. 2009, ApJ, 702, 1615

Cyganowski, C. J., Brogan, C. L., Hunter, T. R., et al. 2012, ApJ, 760, L20

Downes, D., Wilson, T. L., Bieging, J., & Wink, J. 1980, A&AS, 40, 379

Draine, B. T. 2003, ARA&A, 41, 241

Draine, B. T., & McKee, C. F. 1993, ARA&A, 31, 373

Dye, S., Warren, S. J., Hambly, N. C., et al. 2006, MNRAS, 372, 1227

Ellerbroek, L. E., Podio, L., Kaper, L., et al. 2013, A&A, 551, A5

Flower, D. R., & Pineau Des Forêts, G. 2010, MNRAS, 406, 1745

Fox, O., Skrutskie, M. F., Chevalier, R. A., et al. 2009, ApJ, 691, 650

Franco-Hernández, R., & Rodríguez, L. F. 2004, ApJ, 604, L105

Frank, A., Ray, T. P., Cabrit, S., et al. 2014, arXiv, 02, 3553

Froebrich, D., Davis, C. J., Ioannidis, G., et al. 2011, MNRAS, 413, 480

Galván-Madrid, R., Rodríguez, L. F., Ho, P. T. P., & Keto, E. 2008, ApJ, 674, L33

Giannini, T., Calzoletti, L., Nisini, B., et al. 2008, A&A, 481, 123

Giannini, T., Nisini, B., Antoniucci, S., et al. 2013, ApJ, 778, 71

González-Avilés, M., Lizano, S., & Raga, A. C. 2005, ApJ, 621, 359

Guzmán, A. E., Garay, G., Brooks, K. J., & Voronkov, M. A. 2012, ApJ, 753, 51

Hanson, M. M., Luhman, K. L., & Rieke, G. H. 2002, ApJS, 138, 35

Hartmann, L., & Kenyon, S. J. 1996, ARA&A, 34, 207

Hewett, P. C., Warren, S. J., Leggett, S. K., & Hodgkin, S. T. 2006, MNRAS, 367, 454

Hoare, M. G., Kurtz, S. E., Lizano, S., Keto, E., & Hofner, P. 2007, 2007prpl.conf, 181

Hoare, M. G., Purcell, C. R., Churchwell, E. B., et al. 2012, PASP, 124, 939

Hodgkin, S. T., Irwin, M. J., Hewett, P. C., & Warren, S. J. 2009, MNRAS, 394, 675

Hollenbach, D., & McKee, C. F. 1989, ApJ, 342, 306

Hollenbach, D. J., & Tielens, A. G. G. M. 1997, ARA&A, 35, 179

Jones, C., & Dickey, J. M. 2012, ApJ, 753, 62

Kaufman, M. J., & Neufeld, D. A. 1996, ApJ, 456, 611

Keto, E. 2002, ApJ, 568, 754

—. 2003, ApJ, 599, 1196

Keto, E., & Klaassen, P. 2008, ApJ, 678, L109

Keto, E., & Wood, K. 2006, ApJ, 637, 850

Kim, K., & Koo, B. 2001, ApJ, 549, 979

Kolpak, M. A., Jackson, J. M., Bania, T. M., Clemens, D. P., & Dickey, J. M. 2003, ApJ, 582, 756

Koornneef, J. 1983, A&A, 128, 84

Krumholz, M. R., Klein, R. I., & McKee, C. F. 2012, ApJ, 754, 71

Krumholz, M. R., Klein, R. I., McKee, C. F., Offner, S. S. R., & Cunningham, A. J. 2009, Science, 323, 754

Kuiper, R., & Yorke, H. W. 2013a, ApJ, 763, 104

—. 2013b, ApJ, 772, 61

Kurtz, S., Churchwell, E., & Wood, D. O. S. 1994, ApJS, 91, 659

Lada, C. J. 1985, ARA&A, 23, 267

Lawrence, A., Warren, S. J., Almaini, O., et al. 2007, MNRAS, 379, 1599

Le Bourlot, J., Pineau des Forêts, G., Flower, D. R., & Cabrit, S. 2002, MNRAS, 332, 985

Lee, J.-J., Koo, B.-C., Lee, Y.-H., et al. 2014, arXiv, 06, 4271, accepted in MNRAS

Lucas, P. W., Hoare, M. G., Longmore, A., et al. 2008, MNRAS, 391, 136

Moisés, A. P., Damineli, A., Figuerêdo, E., et al. 2011, MNRAS, 411, 705

Mottram, J. C., Hoare, M. G., Davies, B., et al. 2011, ApJ, 730, L33

Mouri, H., & Taniguchi, Y. 2000, ApJ, 534, L63

Neufeld, D. A., & Dalgarno, A. 1989, ApJ, 344, 251

Nisini, B., Bacciotti, F., Giannini, T., et al. 2005, A&A, 441, 159

Nisini, B., Caratti o Garatti, A., Giannini, T., & Lorenzetti, D. 2002, A&A, 393, 1035

Podio, L., Bacciotti, F., Nisini, B., et al. 2006, A&A, 456, 189

Purcell, C. R., Hoare, M. G., Cotton, W. D., et al. 2013, ApJS, 205, 1

Radhakrishnan, V., Goss, W. M., Murray, J. D., & Brooks, J. W. 1972, ApJS, 24, 49

Ray, T., Dougados, C., Bacciotti, F., Eislöffel, J., & Chrysostomou, A. 2007, 2007prpl.conf, 231

Reipurth, B., & Bally, J. 2001, ARA&A, 39, 403

Rieke, G. H., & Lebofsky, M. J. 1985, ApJ, 288, 618

San José-García, I., Mottram, J. C., Kristensen, L. E., et al. 2013, A&A, 553, A125

Shepherd, D. S., & Churchwell, E. 1996, ApJ, 457, 267

Shinn, J.-H., Pyo, T.-S., Lee, J.-J., et al. 2013, ApJ, 777, 45

Skrutskie, M. F., Cutri, R. M., Stiening, R., et al. 2006, AJ, 131, 1163

Thompson, M. A., Hatchell, J., Walsh, A. J., MacDonald, G. H., & Millar, T. J. 2006, A&A, 453, 1003

van der Tak, F. F. S., Tuthill, P. G., & Danchi, W. C. 2005, A&A, 431, 993

Varricatt, W. P., Davis, C. J., Ramsay, S., & Todd, S. P. 2010, MNRAS, 404, 661

Walsh, A. J., Burton, M. G., Hyland, A. R., & Robinson, G. 1998, MNRAS, 301, 640

Waters, L. B. F. M., & Waelkens, C. 1998, ARA&A, 36, 233

Watson, C., Araya, E., Sewilo, M., et al. 2003, ApJ, 587, 714

Watson, C., Churchwell, E., Zweibel, E. G., & Crutcher, R. M. 2007, ApJ, 657, 318

Weingartner, J. C., & Draine, B. T. 2001, ApJ, 548, 296

Wilgenbus, D., Cabrit, S., Pineau des Forêts, G., & Flower, D. R. 2000, A&A, 356, 1010

Wilson, T. L. 1972, A&A, 19, 354

Wood, D. O. S., & Churchwell, E. 1989, ApJS, 69, 831

Wu, Y., Wei, Y., Zhao, M., et al. 2004, A&A, 426, 503

Yorke, H. W., & Sonnhalter, C. 2002, ApJ, 569, 846

Zinnecker, H., & Yorke, H. W. 2007, ARA&A, 45, 481

This preprint was prepared with the AAS LaTeX macros v5.2.

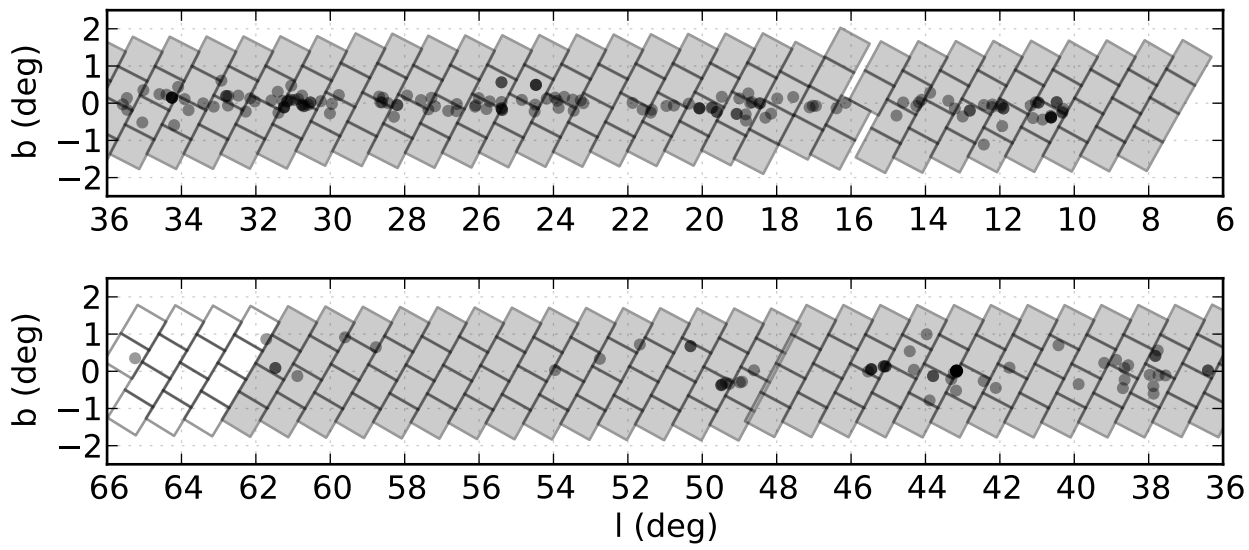

Fig. 1.— Observed area of the UWIFE survey (*grey squares*) and the position of the UCHII (*grey circles*) in the Galactic Coordinates. The position of UCHIIs is from the CORNISH catalog (Purcell et al. 2013). When the positions of circles overlap, the circles appear darker. The two UCHIIs (G061.7207+00.8630 and G065.2462+00.3505) uncovered with the UWIFE survey were separately observed by targeting.

Fig. 2.— Outflow features around CORNISH sources seen in the continuum-subtracted [Fe II] (*top panels*) and RGB composite (*middle panels*; R=H, G=[Fe II], B=H) images. The [Fe II] and H images (FWHM $\sim 0.8''$) are from the UWIFE (Lee et al. 2014) and UKIDSS (Lucas et al. 2008) surveys, respectively. The CORNISH 5 GHz image (FWHM $\sim 1.5''$) is shown for reference in the *bottom-left panel*. The *dashed boxes* in the *left panels* indicate the region enlarged in the *right panels*. Ellipses indicate where the flux is measured (on-source:*solid*, off-source:*dashed*). The ellipse pairs (on+off) are alphabetically tagged in order of increasing RA (cf. *top-right panel*). Circles with a red slash indicate the region excluded during the flux measurement. The measured fluxes are listed in Table 1.

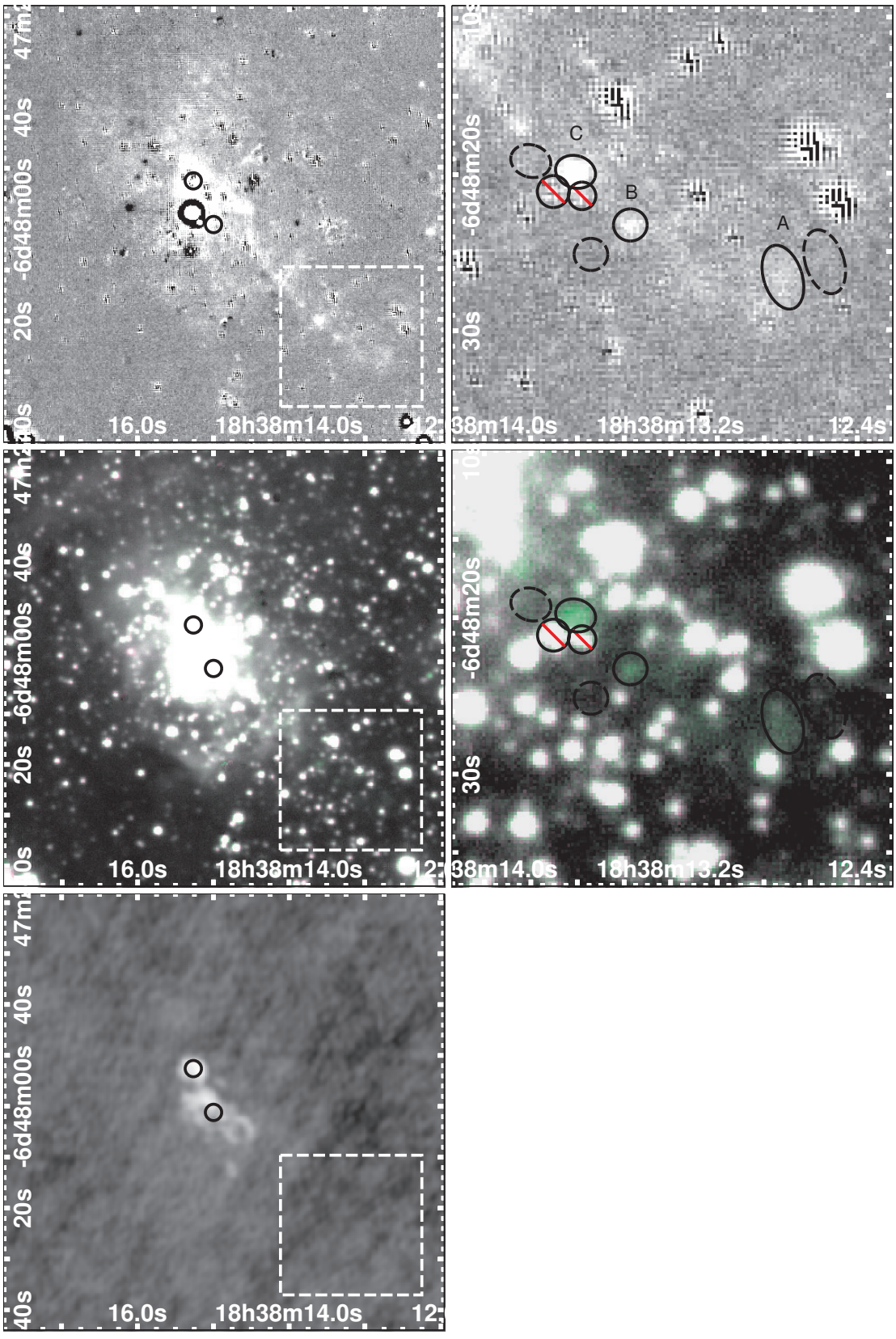

(a) G025.3824−00.1812 (*upper-circle*) and G025.3809−00.1815 (*lower-circle*)

Fig. 2.— (Continued)

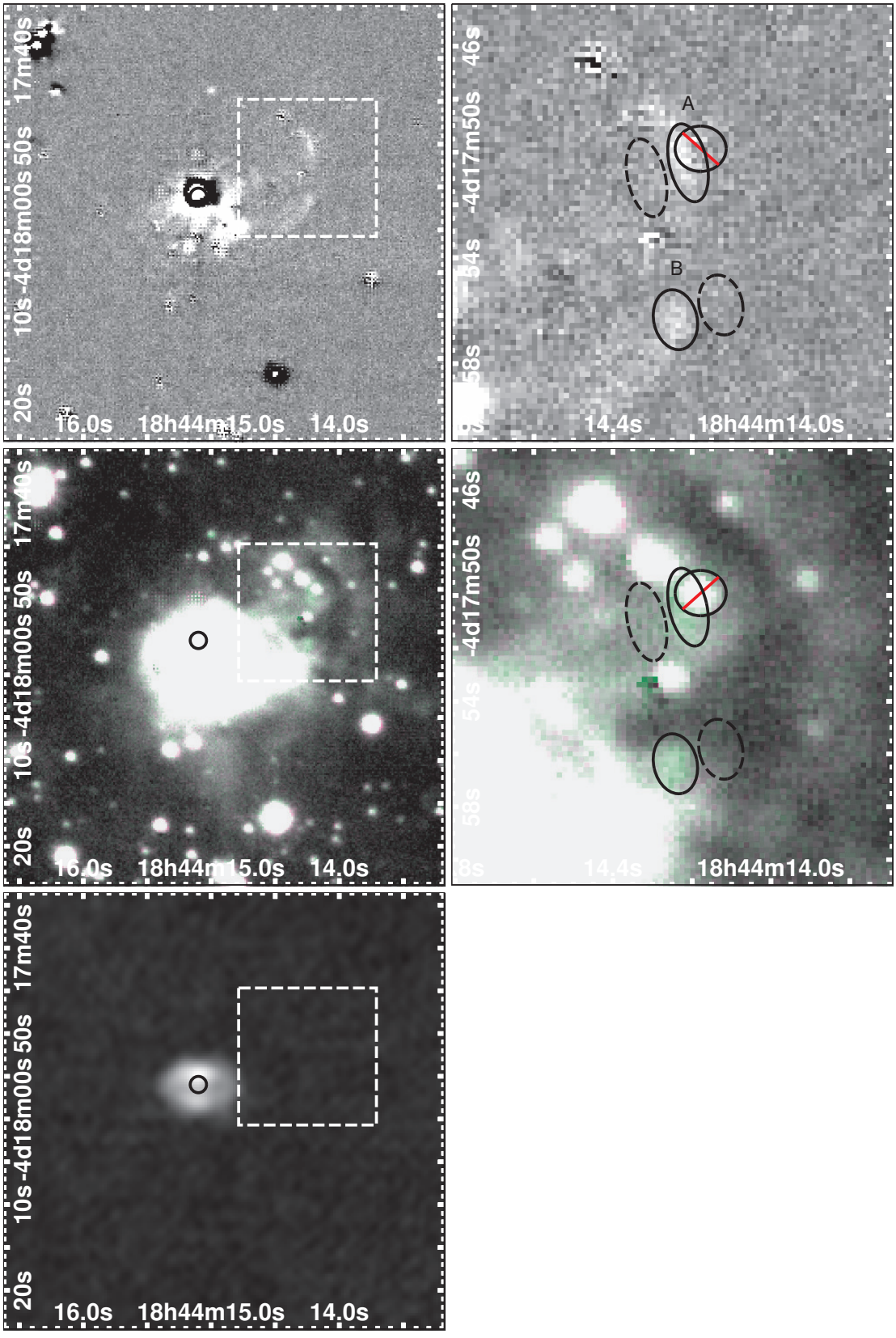

(b) G028.2879−00.3641

Fig. 2.— (Continued)

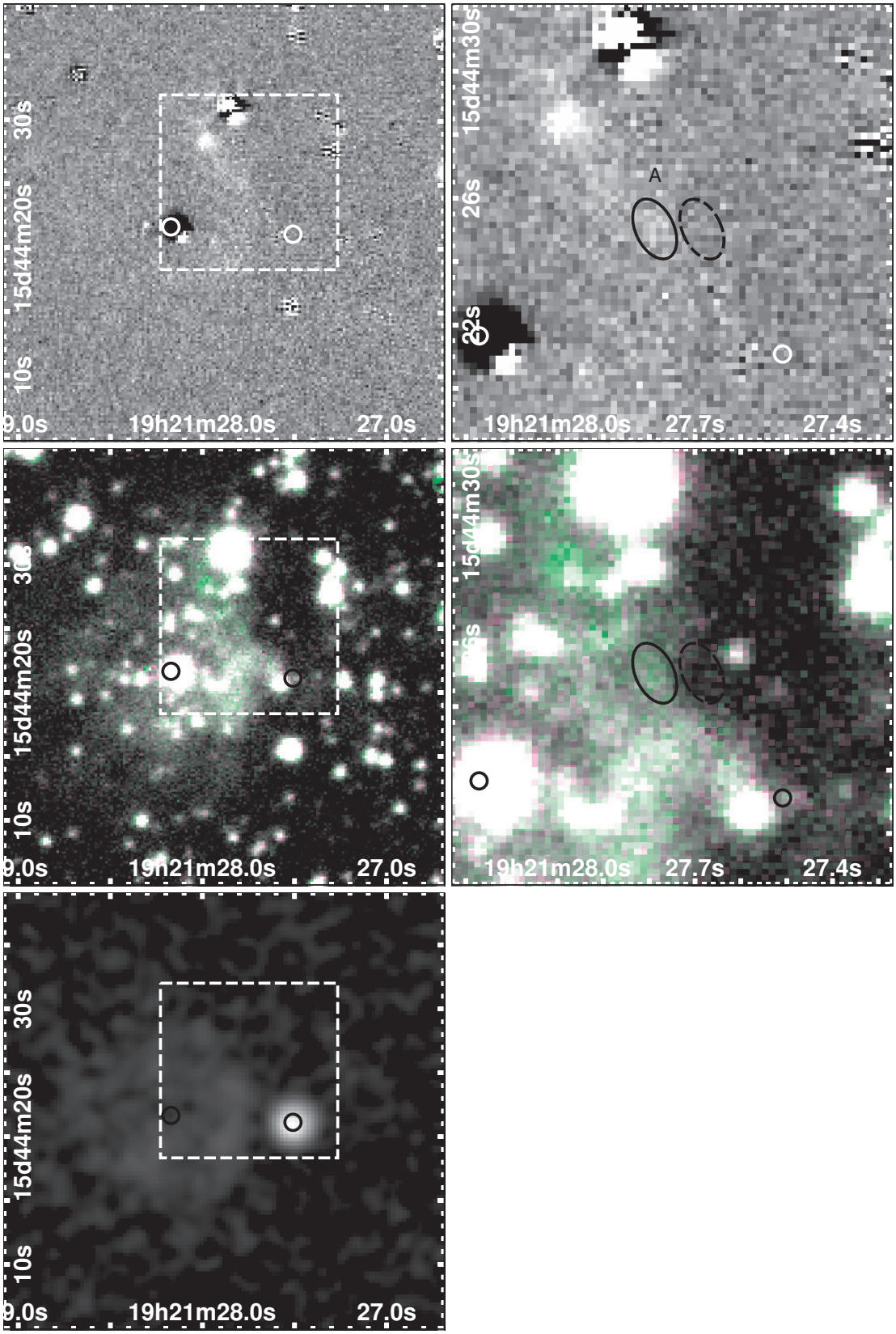

(c) G050.3157+00.6747 (*left-circle*) and G050.3152+00.6762 (*right-circle*)

Fig. 2.— (Continued)

Fig. 3.— Candidate outflow features around CORNISH sources G013.8726+00.2818 seen in the continuum-subtracted [Fe II] (*top*) and RGB composite (*middle*;R=H, G=[Fe II], B=H) images. The candidate [Fe II] features are indicated by arrows for clarity. The [Fe II] and H images (FWHM $\sim 0.8''$) are from the UWIFE (Lee et al. 2014) and UKIDSS (Lucas et al. 2008) surveys, respectively. The CORNISH 5 GHz image (FWHM $\sim 1.5''$) is shown for reference in the *bottom panel*.

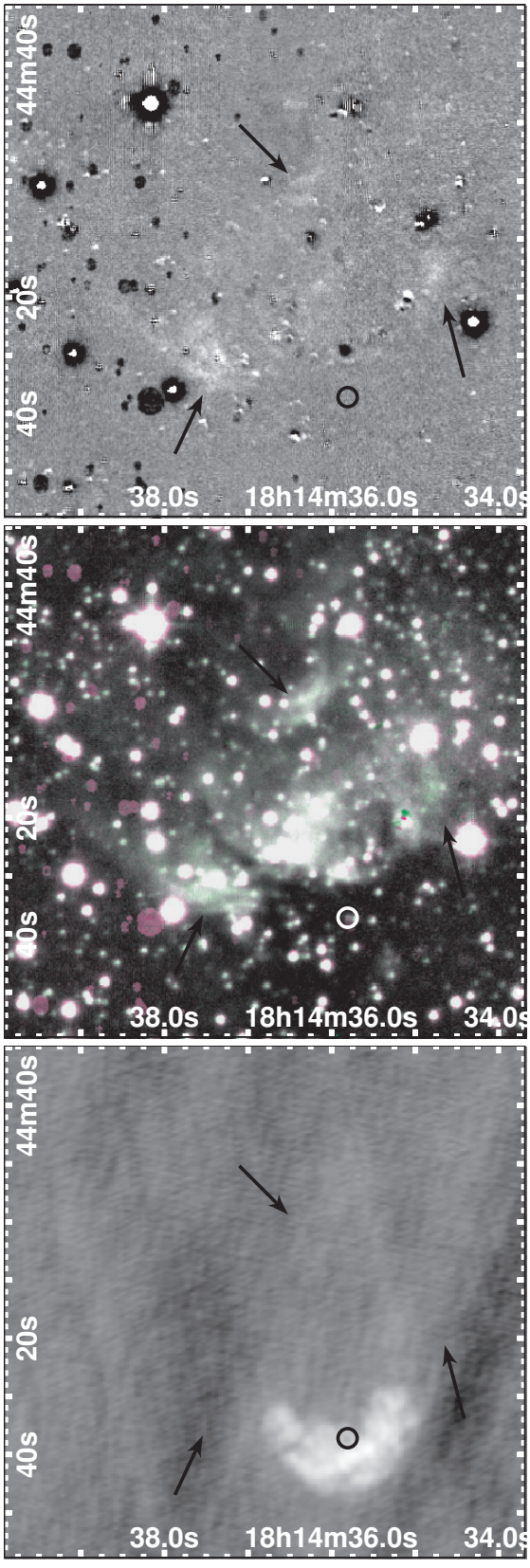

Fig. 3.— (Continued)

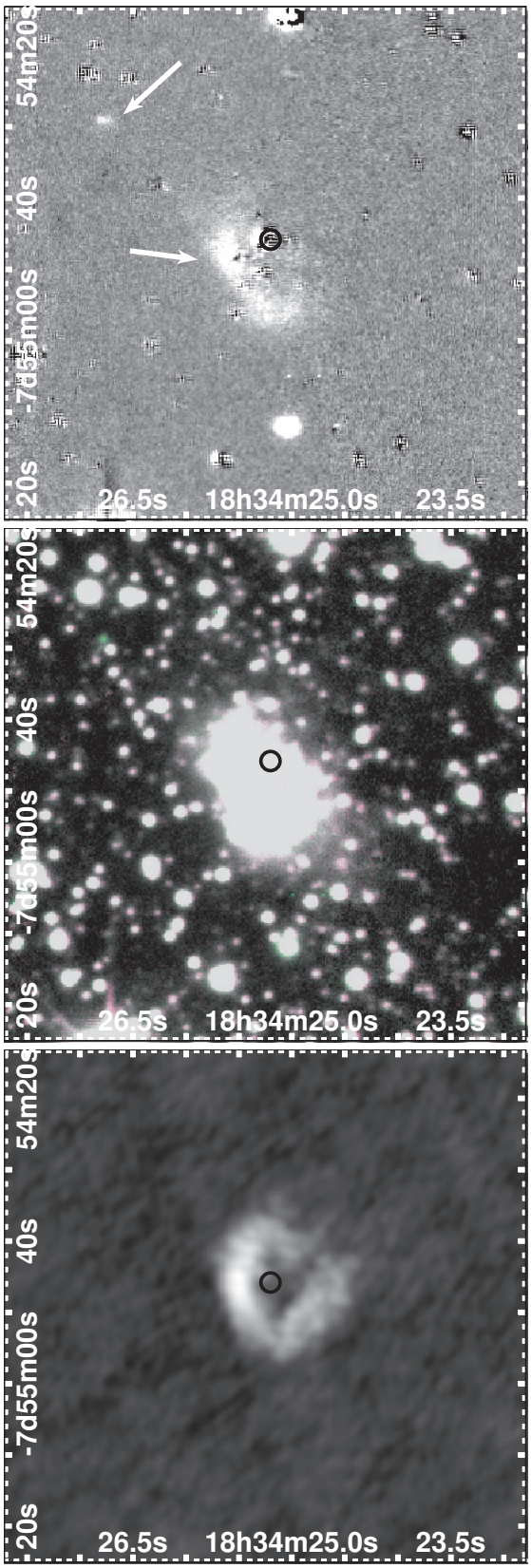

Fig. 4.— The example of excluded [Fe II] features (*arrows*) around UCHII G023.9564+00.1493, seen in the continuum-subtracted [Fe II] image (*top*), RGB composite image (*middle*; R=H, G=[Fe II], B=H), and CORNISH 5 GHz image (*bottom*).

Fig. 5.— Comparison of [Fe II] features with other near-infrared images: the continuum-subtracted [Fe II] (*top-panels*), the H_2 $\upsilon = 1 \rightarrow 0$ $S(1)$ 2.12 μm, K RGB composite image (*middle panels*; R=H_2, G=K, B=K), and the J, H, K RGB composite image (*bottom panel*; R=K, G=H, B=J). The field-of-view setting, boxes, and ellipses are the same as Figure 2. The H_2 (FWHM $\sim 0.7''$) and JHK images (FWHM $\sim 0.8''$) are from the UWISH2 (Froebrich et al. 2011) and UKIDSS (Lucas et al. 2008) surveys, respectively.

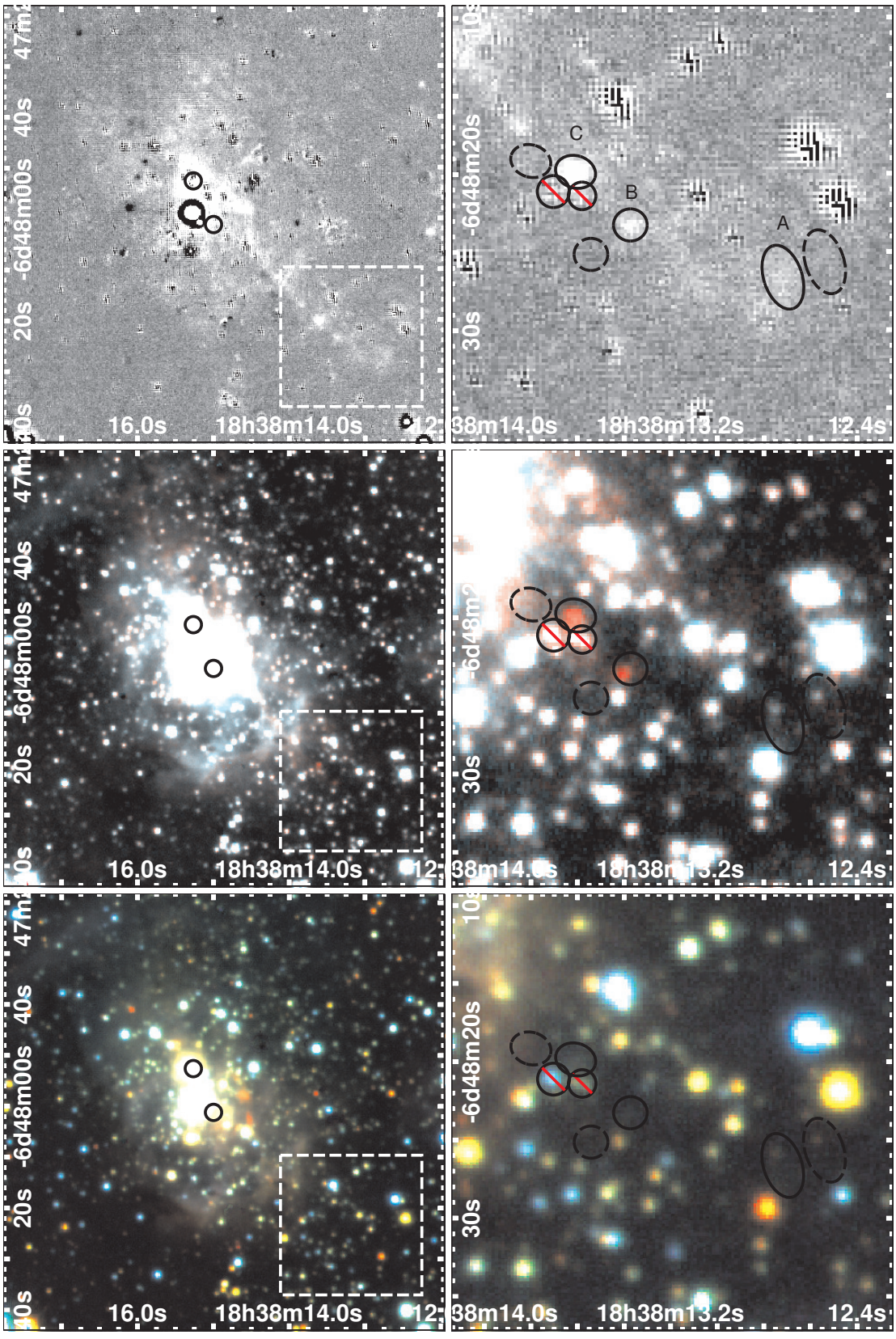

(a) G025.3824−00.1812 (*upper-circle*) and G025.3809−00.1815 (*lower-circle*)

Fig. 5.— (Continued)

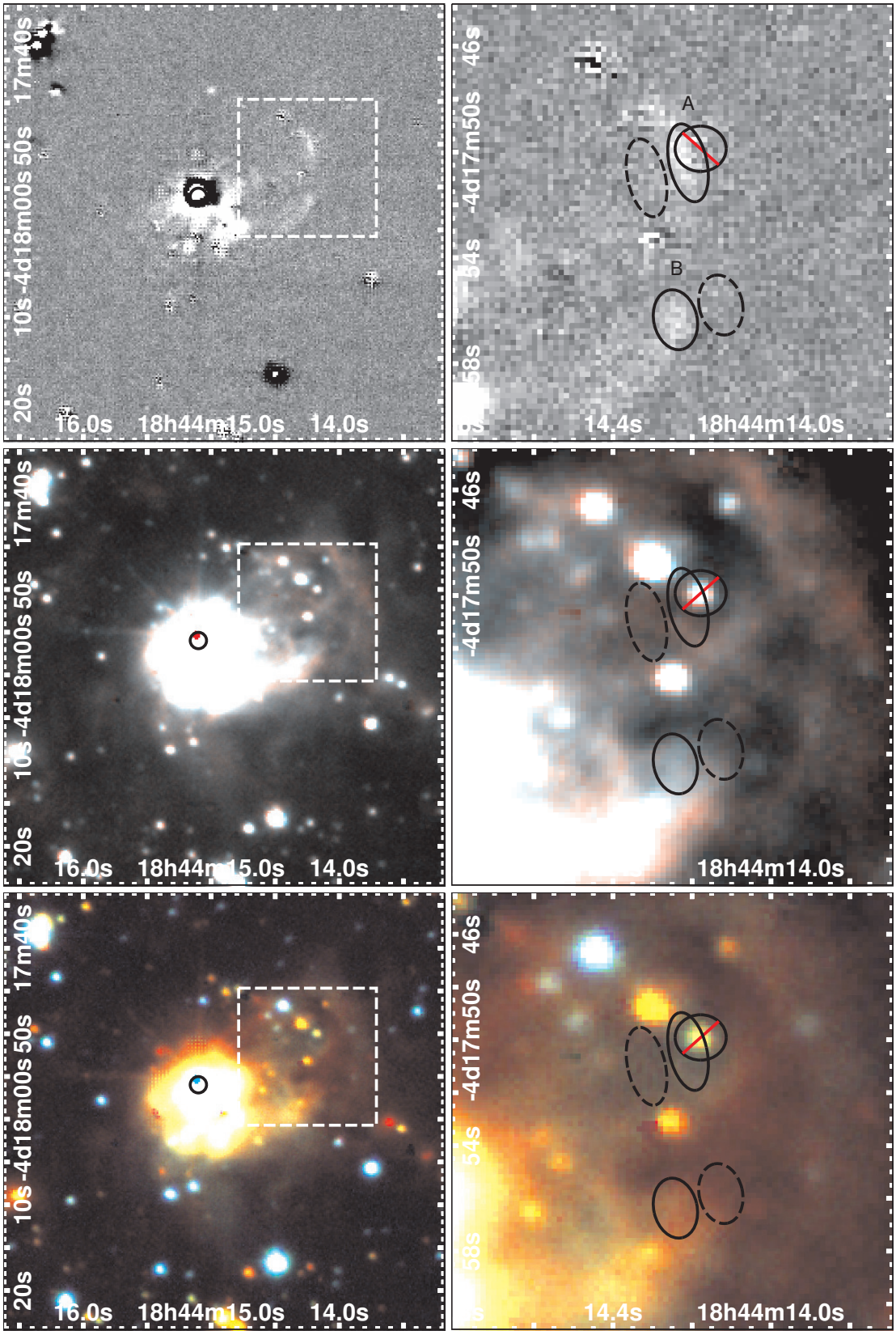

(b) G028.2879−00.3641

Fig. 5.— (Continued)

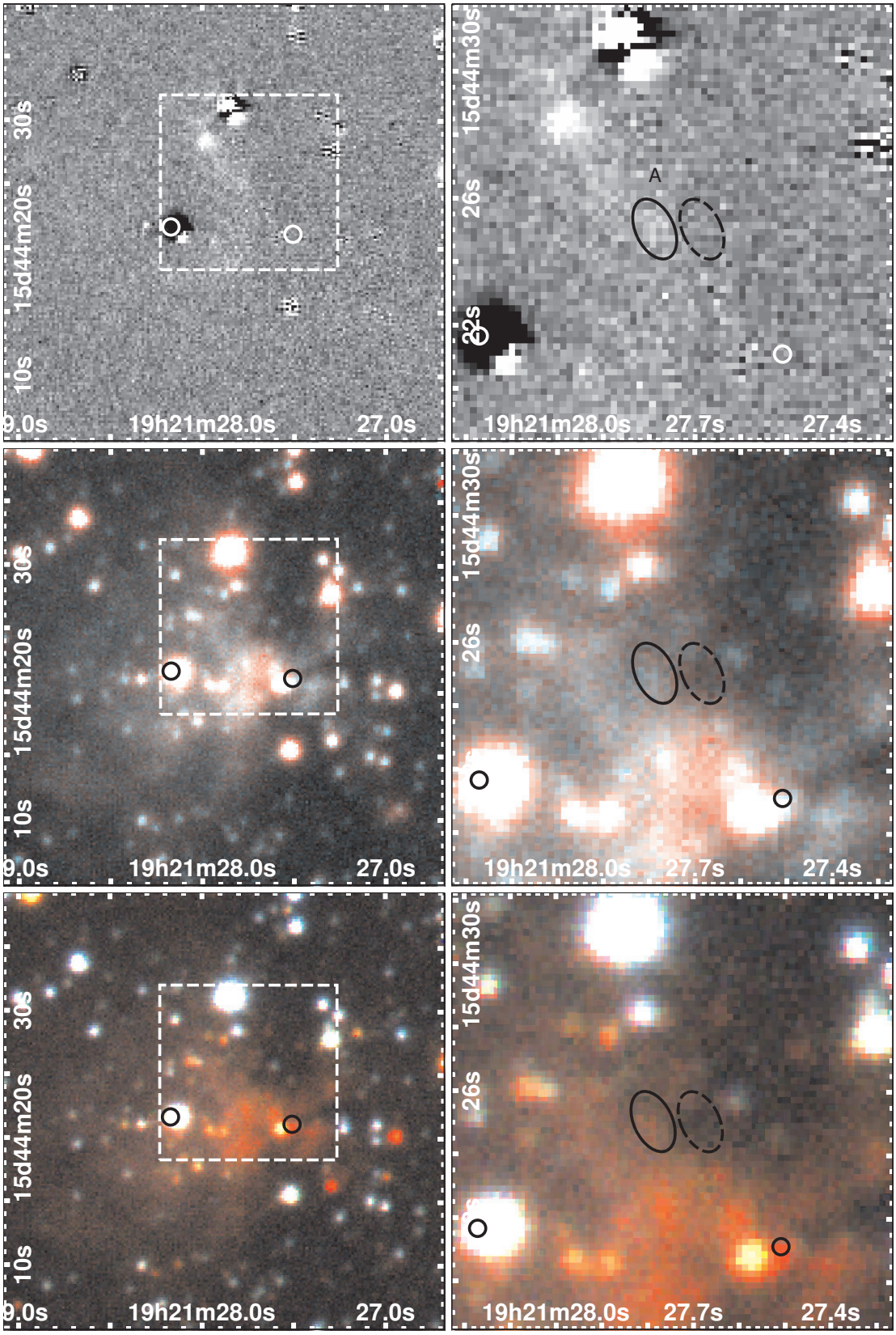

(c) G050.3157+00.6747 (*left-circle*) and G050.3152+00.6762 (*right-circle*)

Fig. 5.— (Continued)

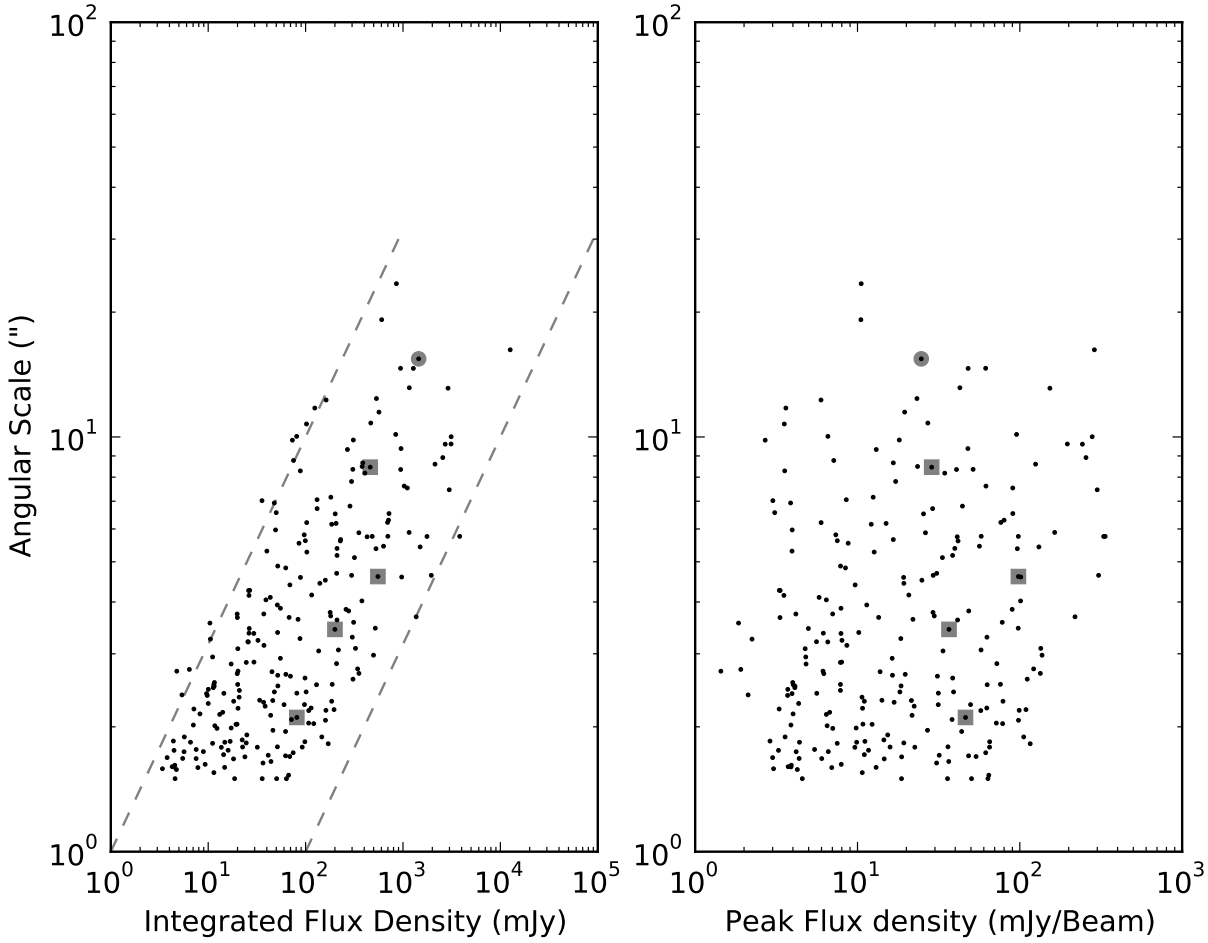

Fig. 6.— The UCHIIs scatter plot using the parameters from the CORNISH UCHII catalog. The *points* are the UCHII candidates from the CORNISH catalog which provides the angular scale, integrated flux density, and peak flux density. The *squares* and *circles* indicate the UCHIIs that show [Fe II] outflow features and candidate features, respectively. The *gray dashed* lines in the *left* plot show the locus of (angular scale) $\sim$ (integrated flux density)$^{1/2}$.

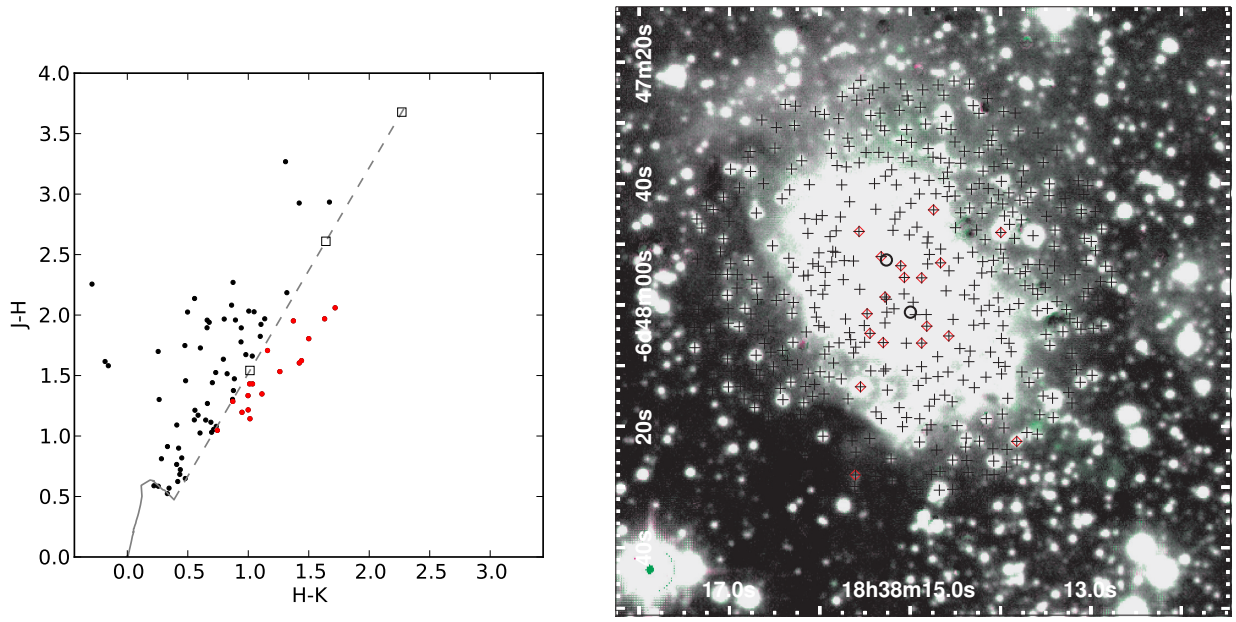

(a) G025.3824−00.1812 and G025.3809−00.1815

Fig. 7.— *left-panels*: color-color diagram. The *points* are the photometry data of the point sources seen in the inspected field. Those points showing infrared excess are colored *red*. The photometry data in the panels (a) and (c) are from the UKIDSS GPS (Lucas et al. 2008). The photometry data in panel (b) are from 2MASS (Skrutskie et al. 2006), since no J-band photometry of UKIDSS GPS is available. The *solid-line* is the locus of main-sequence stars (B9-M6, Hewett et al. 2006). The *dashed-line* is the reddening line (Rieke & Lebofsky 1985), and the *squares* indicate the points that correspond to A_V=10, 20, and 30 from lower-left to upper-right. *right-panels*: RGB composite image of [Fe II] (green) and H (red, blue) as in Figure 2. *crosses* indicate the position of point sources plotted in the color-color diagram (*left-panel*). The point sources showing infrared excess are indicated with *red-diamonds*. The contrast of the image for G025.3824−00.1812 and G025.3809−00.1815 is adjusted to show the [Fe II] features, hence it looks different from Figure 2a.

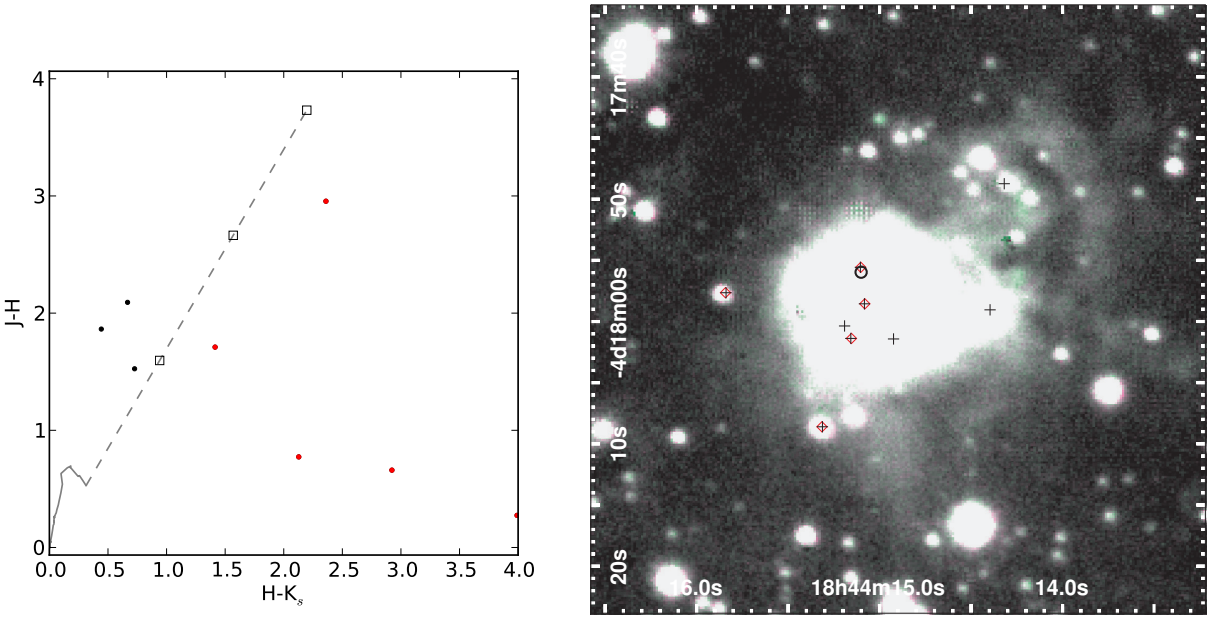

(b) G028.2879−00.3641

Fig. 7.— (Continued)

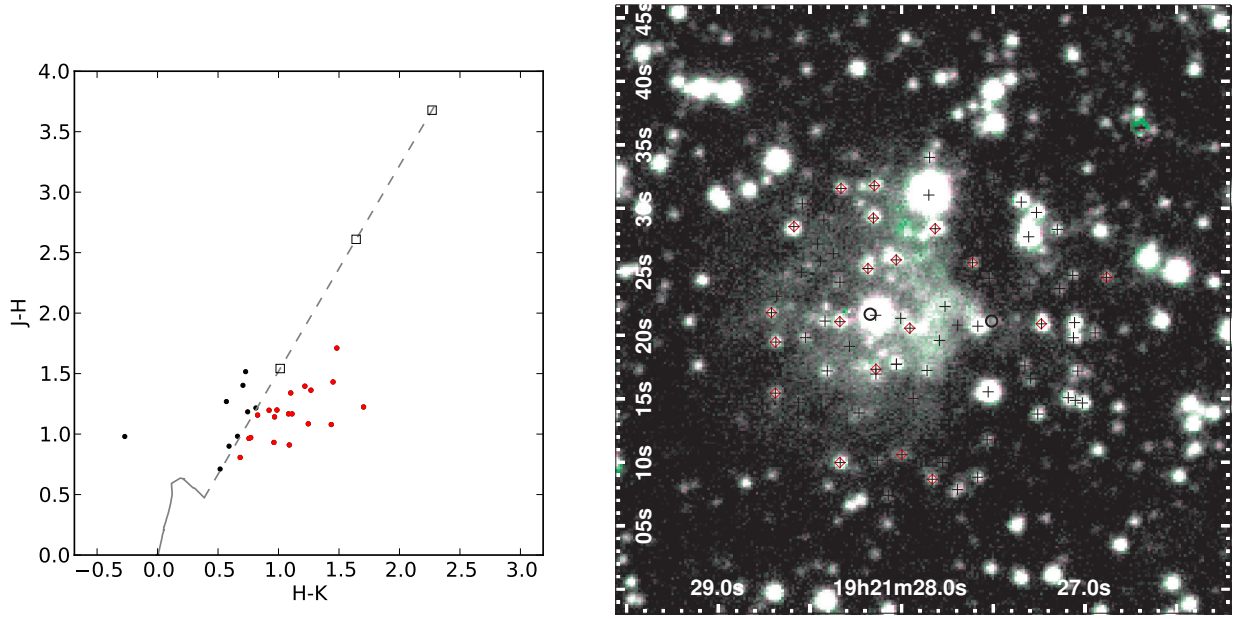

(c) G050.3157+00.6747 and G050.3152+00.6762

Fig. 7.— (Continued)

Table 1. Flux Measurements of [Fe II] Features

Region[a]	RA, Dec (J2000)	A_V[b]	[Fe II] flux	
			Observed	Dereddened[c]
			(10^{-15} erg s^{-1} cm^{-2})	
G025.3809−00.1815-A	18:38:12.719,−6:48:26.63	8.9	5.2±0.2	23.9±0.9
G025.3809−00.1815-B	18:38:13.373,−6:48:23.26	8.9	2.8±0.2	12.6±0.7
G025.3809−00.1815-C	18:38:13.608,−6:48:19.85	8.9	6.6±0.2	30.0±0.9
G028.2879−00.3641-A	18:44:14.210,−4:17:50.44	8.7	2.5±0.1	10.9±0.5
G028.2879−00.3641-B	18:44:14.242,−4:17:56.37	8.7	6.1±0.2	26.6±0.8
G050.3152+00.6762-A	19:21:27.788,+15:44:25.05	20.1	2.2±0.1	65.8±2.4

[a]For simplicity of the region name, we picked one UCHII for the name prefix when there were two UCHIIs relevant to the [Fe II] features.

[b]These values are inferred from near-infrared color excess. See section 3.2 for detail.

[c]The extinctions were corrected, using corresponding A_V and the extinction curve of "Milky Way, $R_V = 3.0$" (Weingartner & Draine 2001; Draine 2003).

Table 2. Outflow Mass Loss Rate Estimated from Dereddened [Fe II] flux

Region[a]	Velocity[b] (km s^{-1})	Distance[c] (kpc)	length ($''$)	Solid Angle (10^{-11} sr)	Method[d]	$\dot{M}_{out}$[e] (10^{-6} $M_\odot$ yr^{-1})
G025.3809−00.1815-A	200	3.9	···	···	Sh	4.44±0.17
G025.3809−00.1815-B	100	3.9	···	···	Sh	16.40±0.90
G025.3809−00.1815-C	100	3.9	···	···	Sh	39.00±1.13
G028.2879−00.3641-A	200	3.2	···	···	Sh	1.36±0.07
G028.2879−00.3641-B	200	3.2	···	···	Sh	3.32±0.10
G050.3152+00.6762-A	200	9.2	1.0	4.3	St	8.87±0.33

[a]For simplicity of the region name, we picked one UCHII for the name prefix when there were two UCHIIs relevant to the [Fe II] features.

[b]We adopted the outflow velocity of 100 km s^{-1} or 200 km s^{-1}. See Section 3.4 for detail.

[c]The distance is adopted from previous estimates. See Section 3.4 for detail.

[d]"Sh" and "St" indicate the "Fe-Shell" and "Fe-Stream" methods used for the $\dot{M}_{out}$ estimation, respectively. See Section 3.4 for detail.

[e]These values are subject to substantial uncertainties originating from the uncertain outflow velocity, extinction, Fe depletion, etc. See the text for details. The listed errors are from the [Fe II] flux error only.

Table 3. UCHII Parameters from the CORNISH Catalog

UCHII	Peak Flux Density (mJy/beam)	Integrated Flux Density (mJy)	Angular Scale (″)	Deconvolved Size (″)
G013.8726+00.2818[a]	24.71±2.21	1447.55±129.84	15.430±0.009	15.4
G025.3809−00.1815	28.64±2.57	460.83±42.66	8.456±0.013	8.3
G025.3824−00.1812	36.62±3.32	200.13±20.03	3.436±0.013	3.1
G028.2879−00.3641	98.00±8.73	552.77±51.90	4.607±0.005	4.4
G050.3152+00.6762	46.28±4.12	81.31±8.07	2.107±0.007	1.5

[a]This UCHII might have [Fe II] features around it, but with a low plausibility (cf. Section 3.1 and Figure 3).

Table 4. Dynamical Time Comparison[a]

UCHII	H II Region Expansion Time (10^3 yr)	Outflow Travel Time (10^3 yr)
G025.3809−00.1815	5.1	4.0−6.1[b]
G025.3824−00.1812	1.9	4.7−7.6[b]
G028.2879−00.3641	2.2	1.0−1.1[b]
G050.3152+00.6762	2.2	1.3

[a]These quantities are estimated with several assumptions. See Section 4.1 for detail.

[b]The time is estimated for all the relevant [Fe II] features (cf. Figure 2).